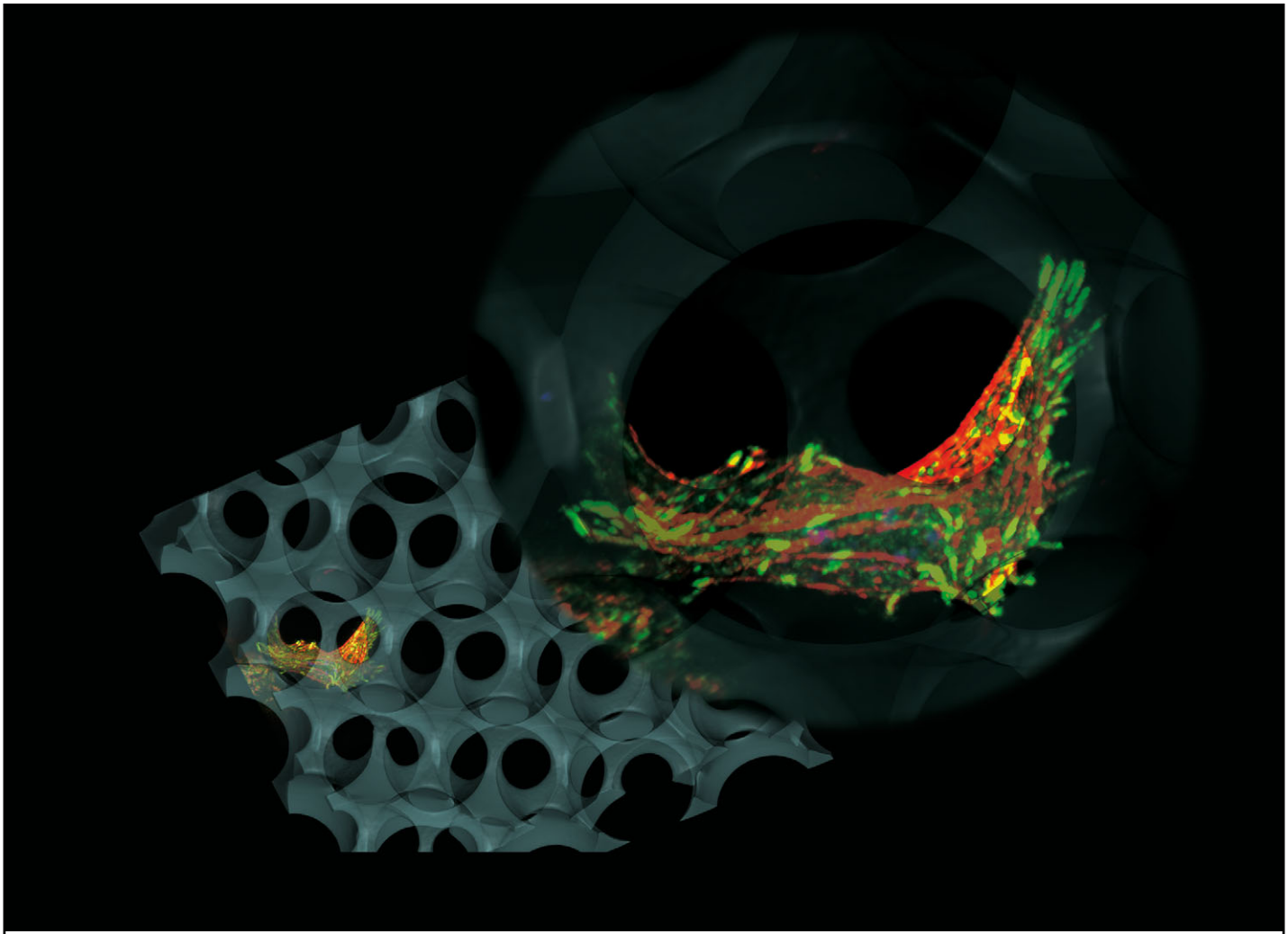

Featuring research from the group of Dr Keng-hui Lin at Institute of Physics, Academia Sinica, Taipei, Taiwan.

Title: Three-dimensional fibroblast morphology on compliant substrates of controlled negative curvature

Lin's lab has engineered a novel 3D culture substrate with tunable stiffness, curvature, and surface coating. The examination of fibroblast morphology grown on the substrates showed that a cell senses local stiffness in 3D and loses its dorsal-ventral asymmetry on a curved substrate.

As featured in:

See Keng-hui Lin *et al.*, *Integr. Biol.*, 2013, **5**, 1447.

RSC Publishing

www.rsc.org/ibiology

Registered Charity Number 207890

Integrative Biology

RSC Publishing

PAPER

View Article Online
View Journal | View Issue

Cite this: *Integr. Biol.*, 2013, **5**, 1447

Three-dimensional fibroblast morphology on compliant substrates of controlled negative curvature†

Yi-hsuan Lee,[a] Jung-ren Huang,[b] Yang-kao Wang[c] and Keng-hui Lin*[a]

Received 30th July 2013,
Accepted 29th September 2013

DOI: 10.1039/c3ib40161h

www.rsc.org/ibiology

Traditionally, cell biological investigations have mostly employed cells growing on flat, two-dimensional, hard substrates, which are of questionable utility in mimicking microenvironments *in vivo*. We engineered a novel scaffold to achieve cell culture in the third dimension (3D), where fibroblasts lose the strong dorsal–ventral asymmetry in the distribution of cytoskeletal and adhesion components that is induced by growth on flat substrates. The design principle of our new 3D substrate was inspired by recent advances in engineering cellular microenvironments in which rigidity and the patterning of adhesion ligands were tuned on two-dimensional substrates; the engineered substrates enable independent control over biochemical and mechanical factors to elucidate how mechanical cues affect cellular behaviours. The 3D substrates consisted of polyacrylamide scaffolds of highly ordered, uniform pores coated with extracellular matrix proteins. We characterized important parameters for fabrication and the mechanical properties of polyacrylamide scaffolds. We then grew individual fibroblasts in the identical pores of the polyacrylamide scaffolds, examining cellular morphological, actin cytoskeletal, and adhesion properties. We found that fibroblasts sense the local rigidity of the scaffold, and exhibit a 3D distribution of actin cytoskeleton and adhesions that became more pronounced as the pore size was reduced. In small pores, we observed that elongated adhesions can exist without attachment to any solid support. Taken together, our results show that the use of negatively curved surfaces is a simple method to induce cell adhesions in 3D, opening up new degrees of freedom to explore cellular behaviours.

Insight, innovation, integration

Designing biomaterials for studying cell–extracellular matrix (ECM) interactions in three dimensions (3D) is key to the biological relevance of observations of cells grown in 3D culture. In recent decades, novel two-dimensional substrates such as compliant gels with patterned proteins have provided many useful insights into how adhesive and mechanical cues drive cellular behavior. Here, we extend cell culture into the third dimension by engineering uniform pores in compliant gels; these pores are treated with fibronectin to pattern ECM proteins as spherical shells. The rigidity of the 3D microenvironment is controlled by the choice of base gels used to assemble the scaffolds. Fibroblasts exhibit quantitative differences in morphology and cytoskeletal architecture following culture in our 3D scaffolds *versus* 2D substrates. Our new technology offers independent control over factors such as three-dimensionality, curvature, biochemical composition, and the mechanical stiffness of the substrate, all of which make critical contributions to the formation of cell adhesions in 3D.

Introduction

Most of our understanding in cell biology has come from cell cultures on flat, two-dimensional (2D), hard substrates. Nevertheless, cells *in vivo* reside within a complex and compliant three-dimensional (3D) microenvironment containing various extracellular matrix (ECM) components. Cells lose their physiological forms when cultured on a simple 2D substrate but regain their physiological forms when cultured by embedding in a 3D matrix.[1] For example, on a 2D substrate, fibroblasts exhibit a flattened morphology and a strong asymmetry in which cellular adhesions are only distributed over the ventral side of the cell surface. When embedded in a 3D matrix, cells display a variety of shapes from stellate to bipolar, lacking a prescribed polarity similar to cell morphology *in vivo*.[2] It has also been shown that cells cultured in 3D have different gene expression levels than their 2D counterparts.[3] An embedded 3D culture is often composed of ECM proteins that self-assemble into a 3D mesh

[a] *Institute of Physics, Academia Sinica, Taipei, Taiwan 11529. E-mail: leey@phys.sinica.edu.tw, kenghui@gate.sinica.edu.tw; Fax: +886-22788-9829; Tel: +886-22789-6763*
[b] *Department of Physics, National Taiwan Normal University, Taipei, Taiwan 11677. E-mail: jrhuang@ntnu.edu.tw*
[c] *Graduate Institute of Biomedical Materials and Tissue Engineering, Center for Neurotrauma and Neuroregeneration, Taipei Medical University, Taipei, Taiwan 110. E-mail: humwang@tmu.edu.tw*

† Electronic supplementary information (ESI) available. See DOI: 10.1039/c3ib40161h

to provide both the mechanical support and the adhesive ligands necessary for the resident cells.[4] Though a 3D matrix mimics the physiological state to some extent, it is hard to dissect the effects of the matrix because a varying matrix gel concentration is often accompanied by simultaneous changes in biochemical, mechanical, and permeation properties. Therefore, it is desirable to design a 3D culture substrate that allows independent control over biochemical and mechanical parameters.

Recent progress in the investigation of cells cultured on 2D substrates of tunable stiffness or with patterned ECM proteins that offer independent control over biochemical and mechanical parameters has advanced our knowledge of how cells interact with their mechanical microenvironment. These substrates are often made of synthetic materials such as elastomers,[5] elastomeric micropost arrays,[6] or hydrogels including polyacrylamide[7] and polyethylene glycol.[8] Substrate stiffness is tuned through the aspect ratio of the micropost or the concentrations of the monomer and the crosslinker in the gels; patterns are generated *via* microfabrication techniques.[9] These studies have demonstrated that various physiological processes, including differentiation,[10] adhesion,[7] migration,[7] proliferation,[11] and apoptosis[12] depend on substrate stiffness and patterning of adhesion ligands. Expanding such synthetic substrates into 3D will empower the investigation of biologically relevant cellular behaviours under controlled conditions.

Of the tunable substrate materials, polyacrylamide gel is the most popular due to its low cost and ease in tuning gels over a wide range of rigidities. Polyacrylamide gel has been used for 3D cell culture *via* strategies such as sandwiching,[13] overlaying,[14] and casting as inverted colloidal crystal scaffolds.[15] However, sandwiching two parallel polyacrylamide substrates over a large area with a gap size of 10 μm is difficult to control.[13] Overlaying a 3D matrix over a 2D polyacrylamide substrate provides adhesion signals from the top and bottom of gels whose rigidity may be very different, with the result that cells may be induced to display non-physiological phenotypes following culture on 2D. Inverted colloidal crystal scaffolds are made by creating large colloidal crystals as templates, infusing the scaffold with polyacrylamide solution, and removing the template colloids. This strategy creates a scaffold of monodisperse pores, but it is time-consuming and costly.

Here we extend a foam-based scaffold fabrication method[16] that is fast and cost-effective for polyacrylamide. First we create a monodisperse liquid foam template using a microfluidic bubble generator, rapidly gel the foam, and open the resulting gelled solid foam through degassing. The simple flow-focusing bubble generator used previously[17] is not readily applicable to hydrogels when gelation requires mixing of chemicals. To overcome this limitation, an *in situ* microbubble-based mixing device is incorporated into our microfluidic device. In this investigation, we characterized important parameters for successful scaffold fabrication and measured the storage moduli (G') of both polyacrylamide gels and scaffolds.

The highly ordered pores of the scaffolds serve as controlled 3D microenvironments with tunable rigidity and spherically distributed adhesive ligands. We are particularly interested in the rigidity sensed by cells cultured in the scaffolds, both in terms of local rigidity in a homogeneous gel and overall scaffold rigidity. We chose fibroblast cells as our model because their morphology and cytoskeletal organization are sensitive to the surrounding rigidity.[13,18] Comparison of fibroblast phenotypes on 2D substrates *vs.* 3D scaffolds yielded critical clues regarding the effective rigidity that cells are able to sense. We also determined that following growth in the small pores of our 3D scaffolds, fibroblasts exhibit very different cytoskeletal and adhesion organization than those following culture on 2D substrates. Given that cellular morphogenesis likely depends on both the geometry and the mechanical properties of the microenvironment, the 3D scaffold is a promising tool for studying cellular morphogenesis in more complex, physiologically relevant environments.

Materials and methods

Fabricating 2D and 3D polyacrylamide substrates

The polyacrylamide precursor solution contained the acrylamide (AC, Bio-rad) monomer, the bisacrylamide (BIS, Bio-rad) crosslinker, the *N*,*N*,*N*′,*N*′-tetramethylethylenediamine (TEMED, Sigma) catalyst, and the Pluronic® F127 surfactant (Sigma) for foam stabilization. The ammonium persulfate (APS, Sigma) initiator was used as the gelling agent. Unless specified, TEMED, APS, and F127 concentration were 0.875%, 0.5%, and 1%, respectively. The AC and BIS ratio is denoted by AC/BIS = w/v%/w/v%. 2D substrates were made by gelling the mixture of precursor solution and the gelling agent in a disc-shaped reservoir of 6 mm in diameter and 1 mm in height.

The 3D substrates were made in a microfluidic device that consisted of a bubble-generating device and a mixing device. Three designs of mixing device were tested (see Results and discussion), and the optimal mixing device was chosen for scaffold fabrication. The device was made of polydimethylsiloxane using standard soft-lithographic techniques.[19] The detailed dimensions of microfluidic devices and bubble-generating conditions are specified in ESI† (Fig. S1 and Table S1). Nitrogen gas (N_2) containing fluorinated molecules, polyacrylamide precursor solution, and the gelling agent were passed through three different inlets (Fig. 1). The monodisperse liquid foam templates were all generated at air fraction ϕ_g = 70%. To shape the scaffolds for cell culture, the liquid polyacrylamide foams were collected in a disc-shaped reservoir and quickly gelled through free radical polymerization. The solid polyacrylamide foams were then degassed under vacuum to become open-pore foams.

For cell culture, the surfaces of polyacrylamide substrates and scaffolds were conjugated with the ECM protein fibronectin (Sigma). The surface ligand density is controlled by the protein concentration during conjugation; when the fibronectin concentration was above 0.5 mg ml^{-1}, the fibroblasts displayed a well-spread morphology on the stiff scaffolds (ESI,† Fig. S2). For all experiments, 0.5 mg ml^{-1} fibronectin was used. The surface modification procedure was similar to previously published methods.[20] Briefly, 20–50 μl of a 1 mg ml^{-1} *N*-sulfosuccinimidyl-6-(4′-azido-2′-nitrophenylamino) hexanoate (sulfo-SANPAH, Thermo) solution were pipetted onto the surface of the polyacrylamide 2D gel or into the 3D scaffold. The polyacrylamide gel or the

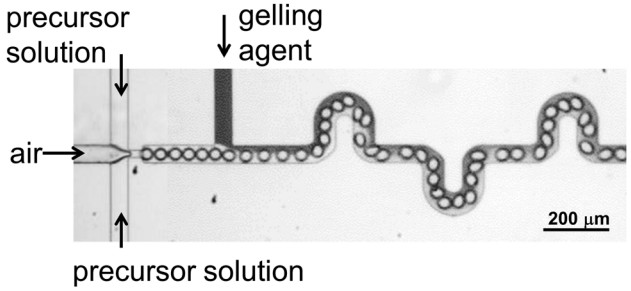

Fig. 1 Optical micrograph of the microfluidic device used to generate the liquid foam template. Bubbles are first generated in a focusing flow containing polyacrylamide precursor solution. The gelling agent (black ink in this image) is introduced into the foam flow and thoroughly mixed with the precursor solution in a series of connected serpentine channels.

scaffold was placed in a UV crosslinker box (CL1000, UVP) for 5 min, then washed with deionized water three times to remove unreacted sulfo-SANPAH. After removing excess water from the gel or the scaffold, 50 μl fibronectin solution (0.5 mg ml^{-1} unless specified) was dropped on top of the polyacrylamide gel or into the scaffold and reacted at 4 °C overnight. We conjugated fibronectin with the Cy5 NHS ester (GE Healthcare) in 0.1 M sodium bicarbonate buffer solution for 2 h to visualize scaffolds. The substrates were then ready for cell culture after several washes in phosphate-buffered saline (GIBCO).

Rheological measurement

We investigated the gelling behaviour of the polyacrylamide solutions and the corresponding polyacrylamide foams and the linear rheology of the polyacrylamide gels and scaffolds using a rheometer (Physica MCR 301, Anton Paar). A disposable parallel plate holder (diameter 25 mm, D-CP/PP7, Anton Paar) with roughened surfaces was used for measurements to avoid slippage. To have better torque resolution in the gelling foam measurements, we used concentric cylinders (C-CC17/T200/AL, Anton Paar). While gelling, all polyacrylamide solutions and liquid foams were subjected to oscillatory shear with a maximum strain of 0.005% at 1 Hz and measured after 30 min to allow complete gellation. For the shear storage modulus (G') of swelling gel and solid foam, the prefabricated gel and solid foam were soaked in water for 24 h to allow swelling, and G' was measured.

Cell culture and immunostaining

NIH 3T3 (ATCC) and Green Fluorescent Protein (GFP)-expressing 3T3 (Cell Biolabs, Inc.) mouse fibroblasts were cultured in Dulbecco's Modified Eagle Medium (GIBCO) supplemented with 10% foetal bovine serum (GIBCO) and 1% penicillin/streptomycin antibiotics (GIBCO) at 37 °C and 5% CO_2. To observe single cell-microenvironment interactions, we seeded a small number of cells (10–20 μl of a cell suspension 10^6 ml^{-1} in density) into the foam scaffolds and onto the 2D polyacrylamide gels.

Cells were immunostained after one day of culture on the substrate. Cells were first fixed with 4% paraformaldehyde (Sigma) in phosphate-buffered saline for 15 min and then permeabilized with 0.2% Triton X-100 in phosphate-buffered saline for 15 min. Mouse anti-paxillin antibody (1 : 100 dilution, BD Bioscience) and Dylight 488 anti-mouse secondary antibody (1 : 200 dilution, Jackson) were used to visualize cell adhesions. Cells were also stained with 33 nM 546 phalloidin (Invitrogen) and 10 μg ml^{-1} Hoechst (Invitrogen) in phosphate-buffered saline for 30 min to visualize F-actin and nuclei, respectively.

Image acquisition and analysis

Stained cells were observed with a 63× glycerol or oil objective on a Zeiss LSM510 or a LSM780 microscope. The images were processed and analyzed using Imaris 7.6.3 (Bitplane). The z spacing was adjusted according to a home-made calibration device (similar to one previously reported[21]) and verified by the spherical shape of the pores. The 3D image stacks were smoothed by the Gaussian filter and segmented by the threshold. Cell shape was quantified using the built-in object-oriented bounding box function, which encloses the cell boundary. The three lengths, l_a, l_b, and l_c, are the principal axes from the shortest to the longest of the minimal volume bounding box (ESI,† Fig. S3). We define l_c as the cell length and $\varepsilon = 1 - \sqrt{l_a l_b}/l_c$ as elongation. The second term describes the ratio of the geometric mean over the cell length. If the cell is perfectly spherical, ε is 0. If the cell is a bipolar spindle with a narrow waist, ε will be close to 1. The value ε is not so sensitive to the threshold value for cell segmentation. When a cell extended very thin filopodia, we only segmented the main body to avoid overestimating ε. For the analysis of paxillin adhesions, the images were first deconvolved by Huygens 4.4 (Scientific Volume Imaging) and threshold. The lengths of paxillin streaks were measured by tracing in Imaris.

Results and discussion

Polyacrylamide scaffold fabrication conditions

In order to consistently produce monodisperse solid foam, the fabrication scheme must meet the following criteria. First, the gelling time (τ_{gel}) for the polyacrylamide mixture must be much shorter than the coarsening time (τ_c) of the foam to maintain the monodispersity of the foam. τ_c sets an upper bound for maintaining monodispersity in our scaffold fabrication process. Second, the duration of the thorough mixing of precursors and gelling reagents in the microfluidic device (τ_{mix}) must be much shorter than the gelation time (τ_{gel}) so that the flow is stable throughout the microfluidic channel.

We investigated how various air compositions affected τ_c.[19] Here, τ_c is the time required for a fraction of hundreds of bubbles to deviate from the average bubble size by more than 10%. For an initial foam of d = 60 μm and ϕ_g = 70%, τ_c was approximately less than 1 min, 3 min, and more than 10 min for bubbles of N_2, N_2 saturated with perfluorohexane (C_6F_{14}) vapour, and hexafluoroethane (C_2F_6) saturated with C_6F_{14} vapour, respectively (Fig. 2). For scaffold fabrication, we used N_2 saturated with C_6F_{14} in the gas phase as an economical choice.

Rapid mixing is a challenging task in microfluidic systems due to the low Reynolds number.[22] Conveniently, introducing bubbles into microfluidic channels significantly enhances local

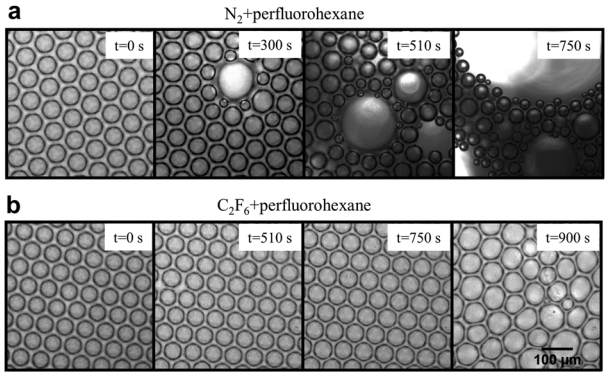

Fig. 2 Micrographs of the evolution of monodisperse foam: (a) N_2 saturated with C_6F_{14} and (b) C_2F_6 saturated with C_6F_{14}.

mixing due to the advection flow at the air–fluid interface.[23] We exploited bubble mixers consisting of a series of repeated mixing channels to ensure thorough mixing. Three designs were tested: branched channels, hexagonal channels, and serpentine channels.[23] A liquid stream containing black ink was used as an indicator to measure the mixing index (MI), which was defined as the standard deviation of the intensity profiles across the channel after each mixing cycle. By this definition, MI equals 0.5 for a 50–50% two-phase flow having a sharp interface, whereas MI equals 0 for a well-mixed flow. Here we defined the time for MI to drop to 0.05 as τ_{mix}. At ϕ_g = 70%, the values of τ_{mix} for the branching, hexagonal, and serpentine channels were 6.3 ms, 14 ms, and 4.1 ms, respectively (Fig. 3). We also found that bubbles could break in the branching channel, an undesirable outcome that led to polydisperse foams. The mixing efficiency of the hexagonal expansion channel decreased substantially with ϕ_g. Overall, the serpentine channel yielded the best performance even at low ϕ_g, and therefore we used this channel design for scaffold fabrication. The mixing efficiency depends on ϕ_g (and hence bubble size). The channel width for the device used for scaffold fabrication was adjusted according to the desired pore size (ESI,† Table S1).

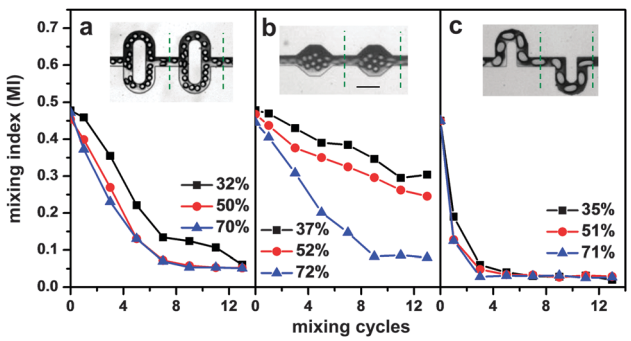

Fig. 3 The mixing indices of three mixing devices. Above, micrographs of the mixing stream in (a) branched, (b) hexagonal, and (c) serpentine channels. The channel width, channel height, and orifice width of all tested devices are 80 μm, 25 μm, and 30 μm, respectively. The scale bar is 200 μm in all micrographs. The dashed lines indicate the MI after each mixing cycle. Below, plots of the mean MI at each mixing cycle for liquid foam flow at various ϕ_g shown in legends in the corresponding mixing channels.

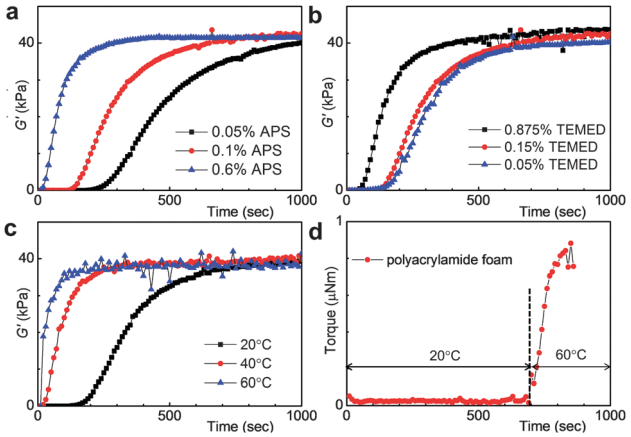

Fig. 4 Storage modulus (G') *versus* time for a homogeneous bulk polyacrylamide mixture containing 10% AC and 0.5% BIS. The mixture was polymerized (a) with 0.15% TEMED and varying amounts of APS at 20 °C, (b) with 0.1% APS and varying amounts of TEMED at 20 °C, and (c) with 0.15% TEMED and 0.05% APS at various temperatures. (d) Polyacrylamide foam containing 10% AC, 0.5% BIS, 0.1% APS, and 0.15% TEMED did not gel until the temperature was raised to 60 °C. All values are presented as time-averaged results.

Rheological measurements provide information on the gelling time and the mechanical modulus of the gel. The storage modulus G' increased as the polyacrylamide mixture polymerized. We defined τ_{gel} as the time required for G' to reach the mid-point of the final plateau value of G_{gel}'. We chose AC/BIS = 10%/0.5% to study the effect of gelling conditions such as temperature, TEMED concentration, and APS concentration on τ_{gel} and G_{gel}'. Polyacrylamide solution gelled faster as the temperature, TEMED concentration, or APS concentration increased (Fig. 4a–c). Raising the temperature was the most effective way to reduce τ_{gel}, and varying these factors did not substantially alter G_{gel}'. Despite identical chemical compositions and reaction conditions, the gelation of polyacrylamide foam was much slower than in its counterpart, homogenous gel (Fig. 4d). The torque change in the polyacrylamide foam gelation measurement was useful to identify conditions in which τ_{gel} was suitable for scaffold fabrication. Polyacrylamide foam mixed with 0.15% TEMED and 0.1% APS did not gel at 20 °C after 10 min, which was much slower than its bulk gelation time (τ_{gel} = 28 s); this foam gelled immediately when the temperature was raised to 60 °C (Fig. 4d). In our hands, 0.875% TEMED and 0.1% APS at 60 °C yielded a moderately fast $\tau_{gel} \sim 60$ s, satisfying the condition $\tau_{mix} \ll \tau_{gel} \ll \tau_c$ to form monodisperse solid foam. Therefore, we used this gelling condition for scaffold fabrication.

Swelling and mechanical properties of polyacrylamide scaffolds

We controlled the microfluidic conditions to produce physically identical liquid foam templates of bubble size d = 60 μm and ϕ_g = 70% for all AC/BIS conditions, but the resulting open-cell foam scaffolds exhibited rather different pore sizes and porosities. The pore sizes of the polyacrylamide scaffolds were approximately 80 μm, 100 μm, and 115 μm for scaffolds of AC/BIS = 12%/0.6%, 12%/0.145%, and 7.5%/0.1%, respectively

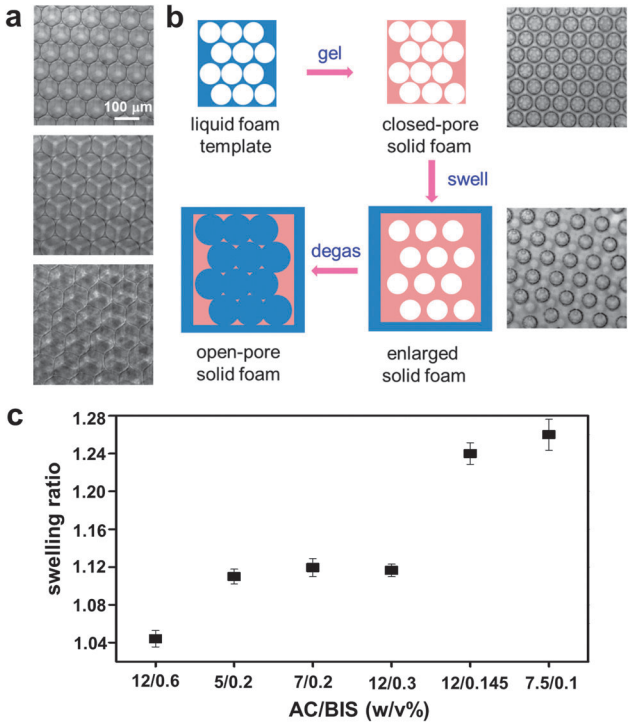

Fig. 5 Swelling effect. (a) Micrographs of polyacrylamide solid foam of hard (top), medium (middle), and soft (bottom) stiffness. (b) Schematic illustrations show that swelling during the fabrication process results in larger pores and higher porosity in the final open-pore solid foam. Right, micrographs of the closed-pore solid foam of AC/BIS = 7.5%/0.1% before (top) and after (bottom) swelling. All micrographs were taken at the same magnification. (c) The swelling ratio of polyacrylamide gels. Each point on the graph is the mean ± standard deviation (n = 10).

(Fig. 5a, top to bottom). These differences in pore size resulted from the combination of two effects: the swelling of the polyacrylamide gel and expansion of the pores by degassing (Fig. 5b). The swelling caused the inter-bubble distance to increase dramatically from the original solid foam (Fig. 5b, micrographs). As the BIS concentration decreased, the degree of swelling increased, and the mechanical strength of the swollen gel decreased.[24] During the degassing process to open the foam, the swollen walls between the pores were irreversibly squeezed by the pressure difference between the inside and the outside of the pore. As a result, in the final open-pore foam the pore diameter was close to the inter-bubble distance in the swollen closed-pore foam (Fig. 5). Therefore, softer scaffolds had larger pores. In order to obtain final scaffolds of the same pore size at different stiffness, we controlled the degree of swelling by choosing an AC/BIS ratio that results in a similar swelling ratio.[25] We found that the AC/BIS concentrations 12%/0.3%, 7%/0.2%, and 5%/0.2% yielded a swelling ratio of 1.12 (Fig. 5c; ESI,† Fig. S4 and Table S2), and therefore we used these concentrations to construct our scaffolds.

We measured G_{sw_gel}' and $G_{scaffold}'$, the respective storage moduli of the homogeneous polyacrylamide gels after swelling and their corresponding scaffolds, and found that these values increased with increases in the concentrations of AC and BIS (Table 1).

Table 1 Storage moduli of polyacrylamide bulks and foams of various AC/BIS

AC/BIS (w/v%)	12/0.6	12/0.3	12/0.145	7/0.2	7.5/0.1	5/0.2
G_{gel}' (Pa)	70 000	36 500	30 000	9130	6140	3080
G_{sw_gel}' (Pa)	52 000	24 900	13 325	5820	3560	2900
$G_{scaffold}'$ (Pa)	6045	2470	1256	780	480	320

The G_{sw_gel}' values were all smaller than the G_{gel}' values due to volume increases from hydration; $G_{scaffold}'$ was usually ~1/10 of G_{sw_gel}'. It is debatable whether the mechanical properties of the local wall in the scaffold are identical to those of the homogeneous gel, because differences may occur due to different reaction conditions and to compaction during degassing. Nevertheless, based on the Gibson–Ashby cellular solid model, the normalized Young's modulus ($E_{scaffold}/E_{sw\_gel}$) of our open solid foam is ~0.09.[26] The normalized storage modulus ($G_{scaffold}'/G_{sw\_gel}'$) should follow a similar ratio, consistent with our data. Thus, the microscopic mechanical properties of the walls in the scaffold should be close to those of a homogenous gel.

The effect of substrate stiffness

$G_{scaffold}'$ was approximately one order of magnitude smaller than G_{sw_gel}' of gels with the same chemical composition (Table 1). When a cell is grown in the scaffold, does it sense the rigidity as measured by the rheometer or sense the local rigidity of the gel? Fibroblasts have been shown to spread into larger areas as the rigidity of the substrate increases.[7,18] Here, we treated the 100 μm pores in our scaffolds as 3D substrates. Cells were cultured on both 2D and 3D substrates made of soft, medium, and hard gels whose AC/BIS ratios were 5%/0.2%, 7%/0.2%, and 12%/0.3%, respectively.

Fibroblasts exhibited similar morphological trends on both 2D and 3D substrates (Fig. 6a). The cells were round on both the soft 2D and 3D substrates, while the cells were more stretched on both the medium substrate and scaffold. We observed that the fibroblasts were even more highly stretched on both the hard substrate and scaffold. To further quantify these differences in cellular morphology, we measured the cell length l_c and elongation ε for more than 30 cells under each cell-culture condition. Generally, l_c and ε increased as the rigidity increased under both 2D and 3D conditions, though the degree of change was more dramatic in 2D cultures (Fig. 6b). For medium gels, l_c and ε were 55 ± 15 μm and 0.67 ± 0.09, respectively, for 2D substrates and 54 ± 13 μm and 0.63 ± 0.09, respectively, for 3D substrates; these respective values were similar to each other in magnitude. For hard gels, l_c and ε were smaller when cells were grown in 3D (83 ± 14 μm and 0.67 ± 0.11 μm, respectively) *versus* 2D (130 ± 38 μm and 0.83 ± 0.06 μm, respectively) because l_c was confined by the pore size d = 100 μm. Surprisingly, for soft gels, l_c and ε were larger in 3D (39 ± 10 μm and 0.61 ± 0.12 μm, respectively) than in 2D (28 ± 9 μm, 0.33 ± 0.16 μm, respectively) substrates. We reason that there are more accessible adhesive sites for round cells to spread on a curved 3D surface than on a flat 2D surface, leading to differences in l_c and ε. Based on this observation, the rigidity sensed by the cells in the scaffold is closer to the local

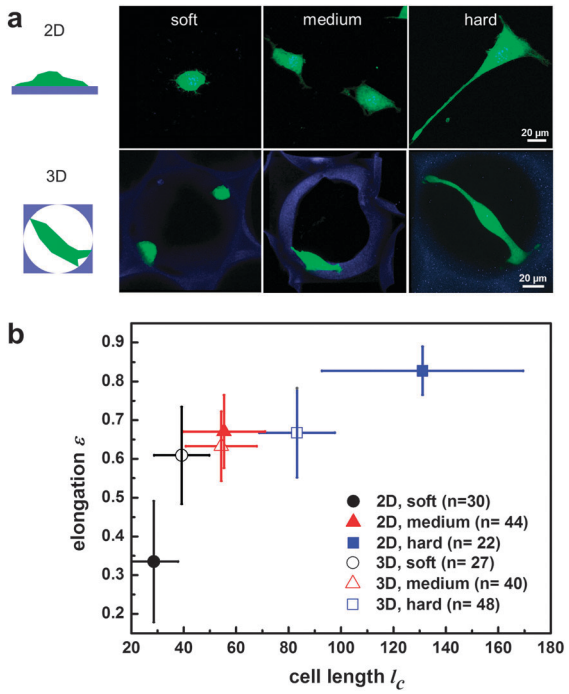

Fig. 6 Elongation of fibroblasts on stiff substrates. (a) Micrographs of fibroblasts on 2D flat substrates (top) and on 3D spherical pores of 100 μm (bottom). Micrographs in the same column are made of the same AC/BIS (5%/0.2%, 7%/0.2%, and 12%/0.3% for soft, medium, and hard gels, respectively). The cell body is shown in green based on expression of whole-body GFP. Fibronectin on the pore surface is labelled with Cy5 (purple) to visualize the pore. (b) The elongation ε *vs.* cell length l_c of cells in scaffolds and on 2D surfaces with different substrate stiffness. Each point on the graph is the mean ± standard deviation.

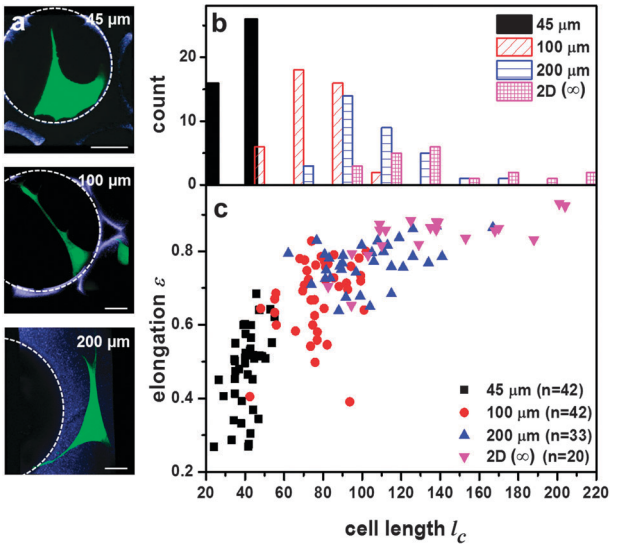

Fig. 7 Pore size confines cell length and elongation. (a) *xy* slices of GFP-expressing fibroblasts in 45 μm, 100 μm, and 200 μm pores (top to bottom). The pore surface is coated with Cy5-labelled fibronectin (purple), and the cells express GFP (green). The scale bar is 20 μm. Histograms of (b) cell length l_c and (c) elongation ε *vs.* l_c of cells in 3D scaffolds and on 2D surfaces.

substrate rigidity (G_{sw_gel}') than to the overall scaffold rigidity ($G_{scaffold}'$); if the cells sensed $G_{scaffold}'$ = 2470 Pa in the hard scaffold, the cell morphology should be more similar to that displayed by cells grown on the soft substrate, which we did not observe. Although non-uniformity in the wall thickness around the pore affects the stiffness sensed by the cell depending on the cell's location, our observations suggest that cells still sense local rigidity in the foam scaffold.

Conventionally, the degree of cell spreading on 2D substrates is assessed by measuring cell area[27] or circumference.[18] The equivalent measurement in 3D is cell surface area, which is very sensitive to the threshold value for cell segmentation. In 3D, l_c and ε are simple quantifications of cell stretching because cell shape is often bipolar. However, ε is not a good indicator if cells are multipolar. For future analyses, we will develop better imaging techniques to improve cell segmentation and to evaluate other cell shapes.

The effect of pore size

The differences in l_c and ε between 3D and 2D substrates prompted us to investigate the effect of pore sizes; scaffolds of uniform, tunable pore size are advantageous in this respect.[28] 3D scaffolds with three pore sizes (d = 45 μm, 100 μm, and 200 μm) were made at AC/BIS = 12%/0.6%. Following 3D culture, fibroblast morphology depended on pore size. At d = 45 μm, fibroblasts tended to form multiple adhesions on each pore, while at d = 100 μm and 200 μm, fibroblasts tended to adopt a long, spindle-like shape (Fig. 7a). We found that pore size limited l_c (Fig. 7b and c). At d = 45 μm, the median l_c was 45 μm, the maximum distance available in the pore, indicating that most cells fully extended their bodies across the pores; the fibroblasts were able to spread more in other directions, decreasing the range of ε. Approximately 90% of cells had ε less than 0.6. At d = 100 μm, median l_c = 77 μm and median ε = 0.68. Less than one-quarter of the cells (10/43) extended more than 90 μm, but nearly half of the observed cells crossed the pore. At d = 200 μm, median l_c = 99.8 μm, and only ~6% (2/34) of cells reached lengths over 150 μm. Most cells conformed to the curved surface and exhibited no confinement in the long axis, yielding ε > 0.6. On a 2D flat substrate, which can be viewed as a pore with d = ∞, the median values of l_c and ε increased to 130 μm and 0.83 μm, respectively.

Organization of F-actin and adhesions

Actin cytoskeleton and adhesions are important cellular machineries for establishing cell shape and for sensing the stiffness of the microenvironment. We observed that the organization of the actin cytoskeleton and the adhesion molecule paxillin depended on substrate rigidity for both 2D and 3D substrates (Fig. 8a). On soft 2D and 3D substrates, actin filaments were concentrated on the periphery or in the cortical regions of the cells; paxillin was distributed diffusively throughout the cell body (Fig. 8a). As 2D substrate stiffness increased, actin filaments became pronounced, appearing as actin stress fibres across the cell body, while paxillin was concentrated in focal adhesion sites (Fig. 8a). On 3D hard substrates, thick actin bundles and paxillin streaks formed that were similar to the actin stress fibres and focal adhesions on the 2D substrate (Fig. 8a). The actin bundles

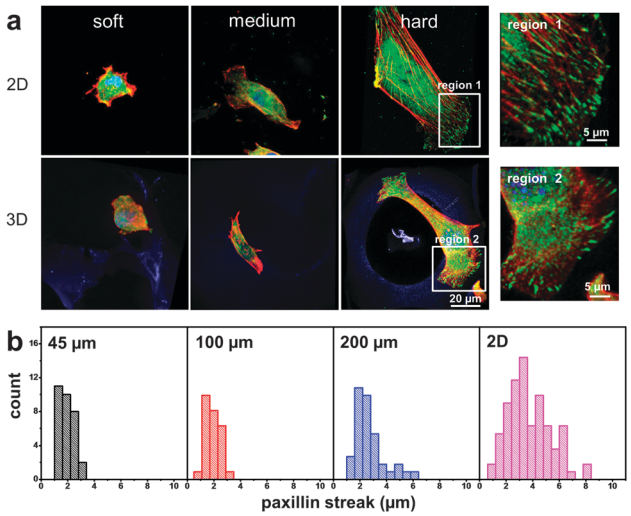

Fig. 8 The distribution of paxillin streaks. (a) Morphology of fibroblasts cultured on 2D substrates (top) and 3D scaffolds (bottom) with different stiffnesses (left to right). Nuclei were stained with Hoescht (blue), f-actin was stained with phalloidin (red), and paxillin was immunolabelled (green). (b) Histograms of the lengths of paxillin streaks of single cells grown in pores of various sizes (data are taken from one cell under each growth condition). Thirty paxillin streaks were observed for d = 45 and 100 μm; 40 streaks were observed for d = 200 μm, and 86 streaks were observed for the 2D substrate ($d = \infty$).

were thinner and less pronounced than the 2D stress fibres, and there were fewer, thinner paxillin streaks in fibroblasts grown in 3D scaffolds (Fig. 8a). The number and size of the paxillin streaks decreased with decreasing pore size (ESI,† Fig. S5). At d = 45 μm and 100 μm, the maximum length of the paxillin streaks was ~3.5 μm, which is less than half of the maximum length of the focal adhesions produced by fibroblasts grown on 2D substrates (Fig. 8b). The similarity in the trends in actin cytoskeleton and adhesion organization displayed by cells grown in 2D and 3D environments support our hypothesis that cells sense local rigidity in a 3D scaffold (Fig. 6).

Dimensionality affected the distributions of the actin cytoskeleton and focal adhesions; these features occurred around the full peripheries of fibroblasts grown in 3D scaffolds, while actin stress fibres and focal adhesions were concentrated on the ventral side of cells cultured on 2D substrates (data not shown), as observed in many previous studies. These effects were more pronounced when d = 45 μm (Fig. 9). The data suggest that when fibroblasts are grown in pores in 3D scaffolds, they lose the typical dorsal–ventral polarity exhibited by cells embedded in a 3D ECM and *in vivo*.[2,29] On some occasions, we observed that paxillin streaks present at the cell surface lacked attachments to any solid support; the surfaces of these cells become cusp-shaped at the locations of the paxillin streaks (Fig. 9 arrows, and Video S1, ESI†).

Although we have not extensively characterized the actin bundles and paxillin streaks displayed by fibroblasts grown in 3D scaffolds, it is useful to consider these observations in light of our knowledge of stress fibres and focal adhesions. The existence and behaviour of stress fibres and focal adhesions in cells grown in 3D culture are under investigation.[30] Here, we observed more pronounced features than previously reported because our scaffolds were more rigid than other 3D cell cultures, which often include reconstituted collagen gel (usually $E < 1600$ Pa).[14,29a] We were surprised to observe focal adhesions without attachment to a solid support, which may have been possible because the cusp shape of these fibroblasts suggests the existence of a structure inside the cell that generates an outward force that counter-balances the strong contractile force produced by the stress fibres. Therefore, the combination of stress fibres and local strong tension allow the maturation of focal adhesions.[31] More work will be carried out to investigate the characteristics of focal adhesion and stress fibres formed in 3D culture. For example, we plan to compare the spatio-temporal organization and compositions of these cellular features with those exhibited by cells grown in 2D cultures. For example, four categories of stress fibers are of interest: dorsal and ventral stress fibres, transverse arcs, and the perinuclear actin cap.[32] However, we note that this classification is based on previous studies on 2D substrates, and may be different to the case of fibroblasts that lack dorsal–ventral asymmetry after growth on 3D scaffolds.

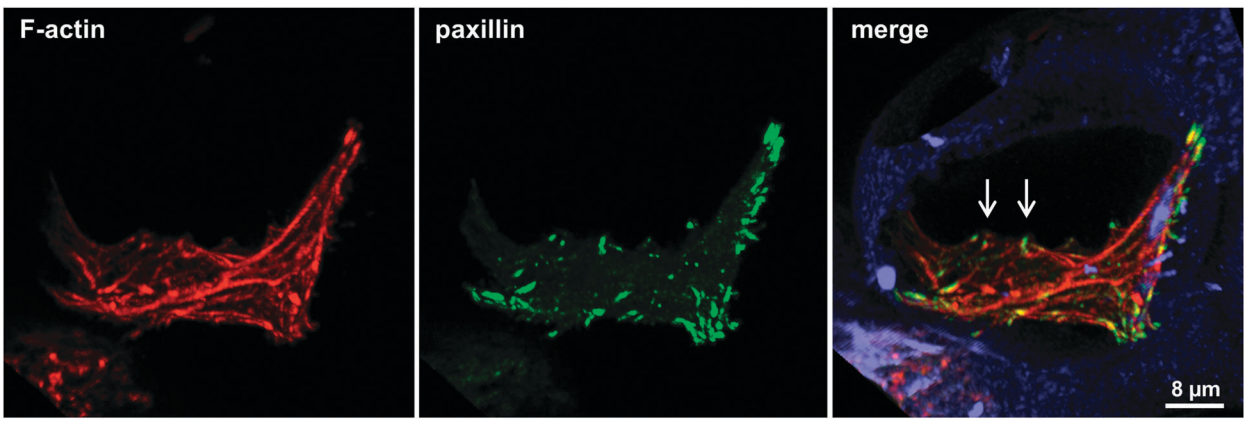

Fig. 9 Cellular features of fibroblasts grown in 3D scaffolds with 45 μm pores. Actin was labelled with phalloidin (red) and paxillin was immunolabelled (green). The merged image (right) includes Cy5-labelled fibronectin (purple) on the surface of pores. The arrows point to the cusps containing paxillin streaks that lack attachment to a solid support.

Conclusion

Here we have demonstrated that the use of a scaffold consisting of uniform pores with tunable rigidity coated with cellular ligands provides more control over the design of biologically relevant microenvironments to direct cellular differentiation and tissue organization in 3D culture. For this purpose, we designed a new microfluidic device for the successful fabrication of polyacrylamide foam scaffolds. We characterized the mechanical properties of polyacrylamide scaffolds and resolved complications associated with gel swelling. Although our scaffolds are ~70% porous and an order of magnitude weaker in mechanical rigidity than a homogenous bulk, we found that fibroblasts grown in these scaffolds sensed the rigidity of their microenvironment as the rigidity of the underlying substrate.

Detailed molecular investigations of the actin cytoskeleton and the distribution of adhesion molecules yielded insight into the behaviour of cells grown in 3D culture. Scaffold pores can be patterned with adhesive ligands to generate negatively curved surfaces that are suitable for establishing cell adhesion in 3D. This radius of curvature occurs at a length scale that is similar to that of the cytoskeleton, and modifies actin bundle organization.[33] We found that the actin bundles were generally thinner and the adhesion streaks were smaller in cells grown in our 3D scaffolds. We speculate that the force exerted by the cell on the surrounding matrix may be weaker than in the 2D scenario, causing smaller focal adhesions when fibroblasts are cultured in 3D. These compliant, negatively curved substrates are readily applicable for traction force measurements, an ongoing project in our lab. The extra spatial dimension available to cells cultured in 3D opens up many degrees of freedom for cell adhesions and cytoskeletal organization that may affect cell stiffness, traction force, and other cell functions; the possible configurations of cell adhesions and stress fibres are confined in 2D. We suggest an analogy with polymer physics in which confinement affects the configurations available to a stiff polymer, thus impacting the polymer's scaling behaviours and elasticity.[34] Our negatively curved substrate offers a simple method for 3D cell culture that will facilitate investigations into the effect of spatial dimensionality on cellular behaviour.

Acknowledgements

This work is supported by NSC 99-2112-M-001-022-MY3 and the Academia Sinica Research Program on Nanoscience and Nanotechnology. Technical support from NanoCore, the Core Facilities for Nanoscience and Nanotechnology at Academia Sinica in Taiwan, is acknowledged. Experiments and data analysis were performed in part through the use of the confocal microscope at the Scientific Instrument Center of Academia Sinica and with the assistance of Shu-Chen Shen. Yi-hsuan Lee acknowledges her postdoctoral fellowship from Academia Sinica.

Notes and references

1 B. M. Baker and C. S. Chen, Deconstructing the third dimension – how 3D culture microenvironments alter cellular cues, *J. Cell Sci.*, 2012, **125**, 3015–3024.
2 F. Grinnell, Fibroblast biology in three-dimensional collagen matrices, *Trends Cell Biol.*, 2003, **13**, 264–269.
3 P. A. Kenny, G. Y. Lee, C. A. Myers, R. M. Neve, J. R. Semeiks, P. T. Spellman, K. Lorenz, E. H. Lee, M. H. Barcellos-Hoff, O. W. Petersen, J. W. Gray and M. J. Bissell, The morphologies of breast cancer cell lines in three-dimensional assays correlate with their profiles of gene expression, *Mol. Oncol.*, 2007, **1**, 84–96.
4 J. Lee, M. J. Cuddihy and N. A. Kotov, Three-dimensional cell culture matrices: State of the art, *Tissue Eng., Part B*, 2008, **14**, 61–86.
5 N. Q. Balaban, U. S. Schwarz, D. Riveline, P. Goichberg, G. Tzur, I. Sabanay, D. Mahalu, S. Safran, A. Bershadsky, L. Addadi and B. Geiger, Force and focal adhesion assembly: a close relationship studied using elastic micropatterned substrates, *Nat. Cell Biol.*, 2001, **3**, 466–472.
6 J. P. Fu, Y. K. Wang, M. T. Yang, R. A. Desai, X. A. Yu, Z. J. Liu and C. S. Chen, Mechanical regulation of cell function with geometrically modulated elastomeric substrates, *Nat. Methods*, 2010, **7**, 733–736.
7 R. J. Pelham and Y. L. Wang, Cell locomotion and focal adhesions are regulated by substrate flexibility, *Proc. Natl. Acad. Sci. U. S. A.*, 1997, **94**, 13661–13665.
8 K. Ghosh, Z. Pan, E. Guan, S. R. Ge, Y. J. Liu, T. Nakamura, X. D. Ren, M. Rafailovich and R. A. F. Clark, Cell adaptation to a physiologically relevant ECM mimic with different viscoelastic properties, *Biomaterials*, 2007, **28**, 671–679.
9 M. Thery, Micropatterning as a tool to decipher cell morphogenesis and functions, *J. Cell Sci.*, 2010, **123**, 4201–4213.
10 A. J. Engler, S. Sen, H. L. Sweeney and D. E. Discher, Matrix elasticity directs stem cell lineage specification, *Cell*, 2006, **126**, 677–689.
11 J. D. Mih, A. S. Sharif, F. Liu, A. Marinkovic, M. M. Symer and D. J. Tschumperlin, A Multiwell Platform for Studying Stiffness-Dependent Cell Biology, *PLoS One*, 2011, **6**, e19929.
12 (*a*) H. B. Wang, M. Dembo and Y. L. Wang, Substrate flexibility regulates growth and apoptosis of normal but not transformed cells, *Am. J. Physiol.: Cell Physiol.*, 2000, **279**, C1345–C1350; (*b*) C. S. Chen, M. Mrksich, S. Huang, G. M. Whitesides and D. E. Ingber, Geometric control of cell life and death, *Science*, 1997, **276**, 1425–1428.
13 K. A. Beningo, M. Dembo and Y. I. Wang, Responses of fibroblasts to anchorage of dorsal extracellular matrix receptors, *Proc. Natl. Acad. Sci. U. S. A.*, 2004, **101**, 18024–18029.
14 M. J. Paszek, N. Zahir, K. R. Johnson, J. N. Lakins, G. I. Rozenberg, A. Gefen, C. A. Reinhart-King, S. S. Margulies, M. Dembo, D. Boettiger, D. A. Hammer and V. M. Weaver, Tensional homeostasis and the malignant phenotype, *Cancer Cell*, 2005, **8**, 241–254.
15 (*a*) Y. J. Zhang, S. P. Wang, M. Eghtedari, M. Motamedi and N. A. Kotov, Inverted-colloidal-crystal hydrogel matrices as

three-dimensional cell scaffolds, *Adv. Funct. Mater.*, 2005, **15**, 725–731; (*b*) J. da Silva, F. Lautenschlager, E. Sivaniah and J. R. Guck, The cavity-to-cavity migration of leukaemic cells through 3D honey-combed hydrogels with adjustable internal dimension and stiffness, *Biomaterials*, 2010, **31**, 2201–2208.

16 K. Y. Chung, N. C. Mishra, C. C. Wang, F. H. Lin and K. H. Lin, Fabricating scaffolds by microfluidics, *Biomicrofluidics*, 2009, **3**, 022403.

17 J.-y. Lin, W.-j. Lin, W.-h. Hong, W.-c. Hung, S. H. Nowotarski, S. M. Gouveia, I. Cristo and K.-h. Lin, Morphology and organization of tissue cells in 3D microenvironment of monodisperse foam scaffolds, *Soft Matter*, 2011, **7**, 10010–10016.

18 T. Yeung, P. C. Georges, L. A. Flanagan, B. Marg, M. Ortiz, M. Funaki, N. Zahir, W. Y. Ming, V. Weaver and P. A. Janmey, Effects of substrate stiffness on cell morphology, cytoskeletal structure, and adhesion, *Cell Motil. Cytoskeleton*, 2005, **60**, 24–34.

19 A. Kabalnov, D. Klein, T. Pelura, E. Schutt and J. Weers, Dissolution of multicomponent microbubbles in the bloodstream: 1. Theory, *Ultrasound Med. Biol.*, 1998, **24**, 739–749.

20 Y. Aratyn-Schaus, P. W. Oakes, J. Stricker, S. P. Winter and M. L. Gardel, Preparation of Complaint Matrices for Quantifying Cellular Contraction, *J. Visualized Exp.*, 2010, e2173.

21 K. E. Jensen, D. A. Weitz and F. Spaepen, Note: A three-dimensional calibration device for the confocal microscope, *Rev. Sci. Instrum.*, 2013, **84**, 016108.

22 G. M. Whitesides and A. D. Stroock, Flexible methods for microfluidics, *Phys. Today*, 2001, **54**, 42–48.

23 (*a*) P. Garstecki, M. A. Fischbach and G. M. Whitesides, Design for mixing using bubbles in branched microfluidic channels, *Appl. Phys. Lett.*, 2005, **86**, 244108; (*b*) A. Gunther, S. A. Khan, M. Thalmann, F. Trachsel and K. F. Jensen, Transport and reaction in microscale segmented gas-liquid flow, *Lab Chip*, 2004, **4**, 278–286; (*c*) X. L. Mao, B. K. Juluri, M. I. Lapsley, Z. S. Stratton and T. J. Huang, Milliseconds microfluidic chaotic bubble mixer, *Microfluid. Nanofluid.*, 2010, **8**, 139–144.

24 K. S. Anseth, C. N. Bowman and L. Brannon-Peppas, Mechanical properties of hydrogels and their experimental determination, *Biomaterials*, 1996, **17**, 1647–1657.

25 J. M. Charest, J. P. Califano, S. P. Carey and C. A. Reinhart-King, Fabrication of Substrates with Defined Mechanical Properties and Topographical Features for the Study of Cell Migration, *Macromol. Biosci.*, 2012, **12**, 12–20.

26 L. J. Gibson and M. F. Ashby, *Cellular Solids*, Cambridge University Press, Cambridge, UK, 2001.

27 B. Amnon, R. Karthikan, E. X. B. Andre' and E. D. Dennis, How deeply cells feel: methods for thin gels, *J. Phys.: Condens. Matter*, 2010, **22**, 194116.

28 (*a*) J. Lee, M. J. Cuddihy, G. M. Cater and N. A. Kotov, Engineering liver tissue spheroids with inverted colloidal crystal scaffolds, *Biomaterials*, 2009, **30**, 4687–4694; (*b*) A. N. Stachowiak and D. J. Irvine, Inverse opal hydrogel-collagen composite scaffolds as a supportive microenvironment for immune cell migration, *J. Biomed. Mater. Res., Part A*, 2008, **85A**, 815–828.

29 (*a*) K. E. Kubow and A. R. Horwitz, Reducing background fluorescence reveals adhesions in 3D matrices, *Nat. Cell Biol.*, 2011, **13**, 3–5; (*b*) R. S. Fischer, M. Gardel, X. F. Ma, R. S. Adelstein and C. M. Waterman, Local Cortical Tension by Myosin II Guides 3D Endothelial Cell Branching, *Curr. Biol.*, 2009, **19**, 260–265.

30 J. S. Harunaga and K. M. Yamada, Cell-matrix adhesions in 3D, *Matrix Biol.*, 2011, **30**, 363–368.

31 P. W. Oakes, Y. Beckham, J. Stricker and M. L. Gardel, Tension is required but not sufficient for focal adhesion maturation without a stress fiber template, *J. Cell Biol.*, 2012, **196**, 363–374.

32 S. Tojkander, G. Gateva, G. Schevzov, P. Hotulainen, P. Naumanen, C. Martin, P. W. Gunning and P. Lappalainen, A Molecular Pathway for Myosin II Recruitment to Stress Fibers, *Curr. Biol.*, 2011, **21**, 539–550.

33 M. A. Schwartz and C. S. Chen, Deconstructing Dimensionality, *Science*, 2013, **339**, 402–404.

34 T. Odijk, On the statistics and dynamics of confined or entangled stiff polymers, *Macromolecules*, 1983, **16**, 1340–1344.